Multi-parameter elastic full-waveform inversion based on the time-lapse VSP Snowflake data

Xiaohui Cai, Kris Innanen, Qi Hu, Don Lawton

ABSTRACT

Vertical seismic profile (VSP) is one of the technologies for monitoring hydrocarbon production and CO_2 geosequestration. We present a workflow of three-parameter elastic full-waveform inversion (EFWI) applied to VSP field data to identify and estimate time-lapse changes introduced by injection of CO_2 at 300 m depth. Application of this workflow to the Snowflake field data shows that EFWI is able to detect and quantify the time-lapse anomaly in P wave velocity with the magnitude of 130-210 m/s.

INTRODUCTION

The significance of monitoring CO_2 can be encapsulated in its critical role within various domains. Monitoring CO_2 levels is paramount due to its substantial impact on climate change and the environment. With rising concerns about global warming, monitoring CO_2 emissions has become crucial in assessing and mitigating its adverse effects. Additionally, in industrial applications such as carbon capture and storage (CCS) or enhanced oil recovery (EOR), precise monitoring of CO_2 injection and its behavior underground is indispensable for ensuring operational efficiency and environmental safety. The data derived from CO_2 monitoring also plays a pivotal role in scientific research, policy-making decisions, and efforts to achieve sustainable practices to combat climate change. Hence, monitoring CO_2 levels is pivotal for understanding its implications on both the environment and human activities, facilitating informed decision-making and proactive measures to address its impacts.

FWI is now regularly used for quantitative assessing images of structures under complex geological conditions (Virieux and Operto, 2009; Pan et al., 2019; Keating and Innanen, 2019; Eaid et al., 2020; Hu et al., 2023), and it makes use of the waveform information, gradually approximating plausible high-resolution models by matching field and simulation data. There are several published examples of successful FWI applications to VSP data (Charara et al., 1996; Owusu et al., 2016), and these VSP-FWI applications for seismic monitoring (Egorov et al., 2017). Currently, the key application of EFWI to land data includes the establishment of initial models and the suppression of cross-talk among multiple parameters. Compared to surface data, the VSP data typically contain more transmitted wave information, which aids in reconstructing low-wave number information in the model, and it generally provides corresponding well-logging data, which could provide a reliable starting model and a constraint on velocity changes to suppress of cross-talk.

In 2018 (Hall et al., 2019) and again in 2022 (Innanen et al., 2022), researchers from the University of Calgary CREWES project (Consortium for Research in Elastic Wave Exploration Seismology) and various external partners collaborated with Carbon Management Canada (CMC) at their Newell County Facility in Alberta, Canada, to acquire baseline and monitoring VSP datasets near a point of injection of CO_2. In the study reported here, we

use EFWI based on three-component accelerometer VSP data for the baseline and monitoring surveys to detect and quantify the time-lapse anomaly in elastic parameters (V_{p} (compressional velocity), V_{s} (shear velocity) and the ρ (density)) with the magnitude.

FIELD DATA INVERSION

Background

Generally, the goal of processing field data for FWI is to prepare data that matches the simulation data, and minimal processing is sufficient. We extract shots from line 4 of the 2018 CMC Newell County Facility field data, called Snowflake, and line 4 is chosen because the injection and observation wells are located on this line, which provides a better basis for research on time-lapse data monitoring of CO_2. As shown in Figure 1, shots from line 4 are located from northeast to southwest. Observation well 2 is located at the center of the shot points, while the injection well is located at the northeast of observation well 2 at a distance of 20 m. Line 4 has a maximum offset of 390 m on the northeast and 480 m on the southwest of observation well 2. Each shot is assigned a 5-digit point number; the first two digits are the line number, and the last three are the shot number. The shot on the northeast edge of line 4 is number 110, and the 82 shots almost increase for 10-meter shot spacing. It appears that the 2022 Snowflake data, depicted in Figure 2, displays a line 4 that closely resembles the corresponding line from the 2018 Snowflake data.

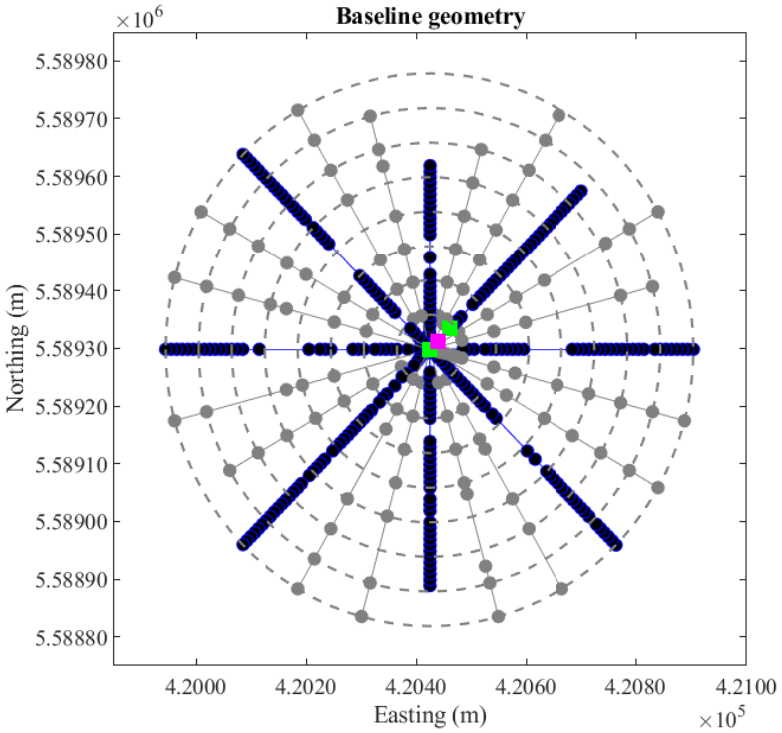

FIG. 1. Baseline shots geometry.

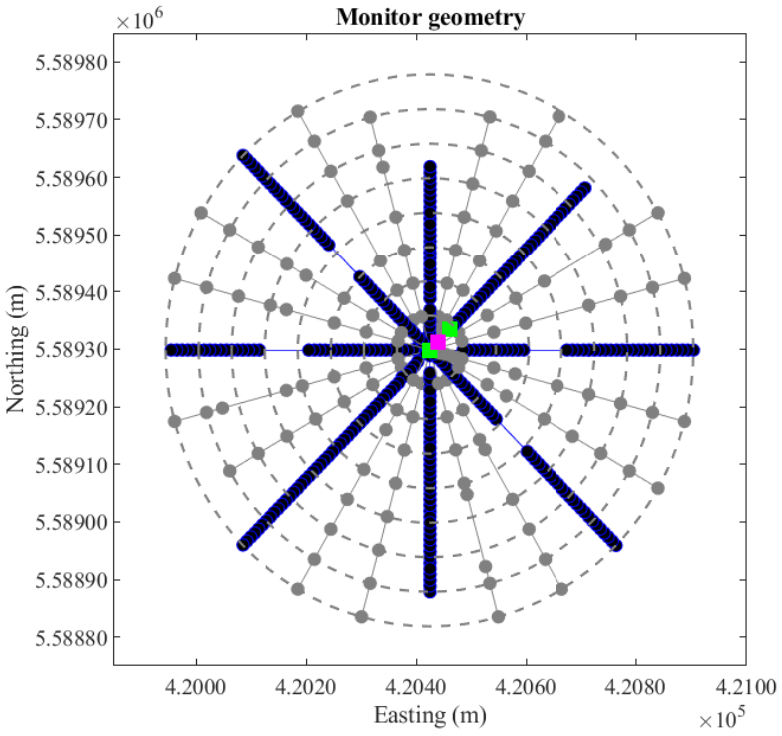

FIG. 2. Monitor shots geometry.

Dataset overview

The trace spacing for the 2018 accelerometer receivers experienced a change from 1 meter (across the interval of 0 meters to 266.4 meters) to 2 meters (from 266.6 meters to 324.2 meters). In contrast, the spacing for the 2022 accelerometer receivers transitioned from 1 meter (spanning 0 meters to 140.3 meters) to 2 meters (from 140.3 meters to 324.2 meters). Most of the signal occurs in the first 500 ms of the dataset; the data are windowed to the first 500 ms.). In the field, the well-log data were interpreted by the soft-sand model and Gassmann's equations (Hu and Innanen, 2019) to provide P-wave sonic, S-wave sonic, and density logs from the surface to 223 m of the injection well, and that above information from 224 m to the bottom of the injection well is acquired by well logs. The accelerometer field data consists of the three orthogonal components of particle acceleration associated with the propagating wavefield. However, the horizontal components are orientated in an unknown, arbitrary direction that varies for each receiver. To ensure that the horizontal data for each receiver has a consistent azimuth, a coordinate rotation needs to be applied to each receiver. The maximum horizontal (Hmax) component is more coherent than the H1 and H2 components and consists of clear downgoing P-wave and S-wave energy and reflections. Therefore, we use the QC Hodogram Display by Vista to rotate the H1 and H2 components to the Hmax and minimal horizontal components. Then, we implement QC rotation angles and adjust the polarity traces individually. Dead traces are replaced through interpolation, and a Butterworth filter (6 Hz to 75 Hz) is applied to accelerometer data. Finally, acceleration is transformed into displacement via -180^o phase transformation. Figure 3 displays the minimally processed 2018 baseline data, while Figure 4 illustrates the

corresponding 2022 monitoring data. In Figure 5, the differences between the monitoring data and baseline data are depicted, revealing clear evidence of distinct upgoing data.

In theory, the injection of CO_2 into the formation is expected to change the elastic parameters, resulting in noticeable changes in the difference between the shot gathers before and after the injection. This change typically manifests as distinct upgoing wavefield data. To derive the synthetic data difference, we consider the logging velocity within this region as the real baseline linear velocity model (shown in Figure **??**). We establish the monitoring velocity model by reducing the $V_{\rm p}$ by 300 m/s, $V_{\rm s}$ by 100 m/s, and the ρ by 50 kg/m^3 at a logging velocity of 300 m (shown in Figure **??**). To simulate the forward propagation for the above two models, we utilize a Ricker wavelet with a dominant frequency of 30 Hz as the seismic source. This enables the second-order accurate forward simulation with a spatial interval of 5 m of the two velocity models. Figure 7 exhibits the difference between the actual monitoring data and the baseline data by these synthetic simulations. Despite some dispersion in the data, observations indicate that the difference in P waves is predominantly concentrated in the vertical component. In contrast, the difference in S waves is primarily evident in the horizontal component. Furthermore, an observable upgoing wavefield ascends to a depth of 300 meters before traveling back to the downgoing wavefield. Because the total length of the detector points is 324 m, the synthetic difference data is mainly the upgoing wave field. Based on the described phenomenon, we execute the separation of the upgoing and downgoing wavefields using FK (frequency-wavenumber) filtering for the field difference data depicted in Figure 5. The separated difference upgoing wavefield is shown in 8. Upon comparing Figure 7 and Figure 8, it becomes evident that the section displaying the upward wave field in the synthetic difference data shot set corresponds noticeably with a prominent upward wave field in Figure 8. Therefore, we update the monitoring data by combining the baseline data with the separated upgoing wavefields.

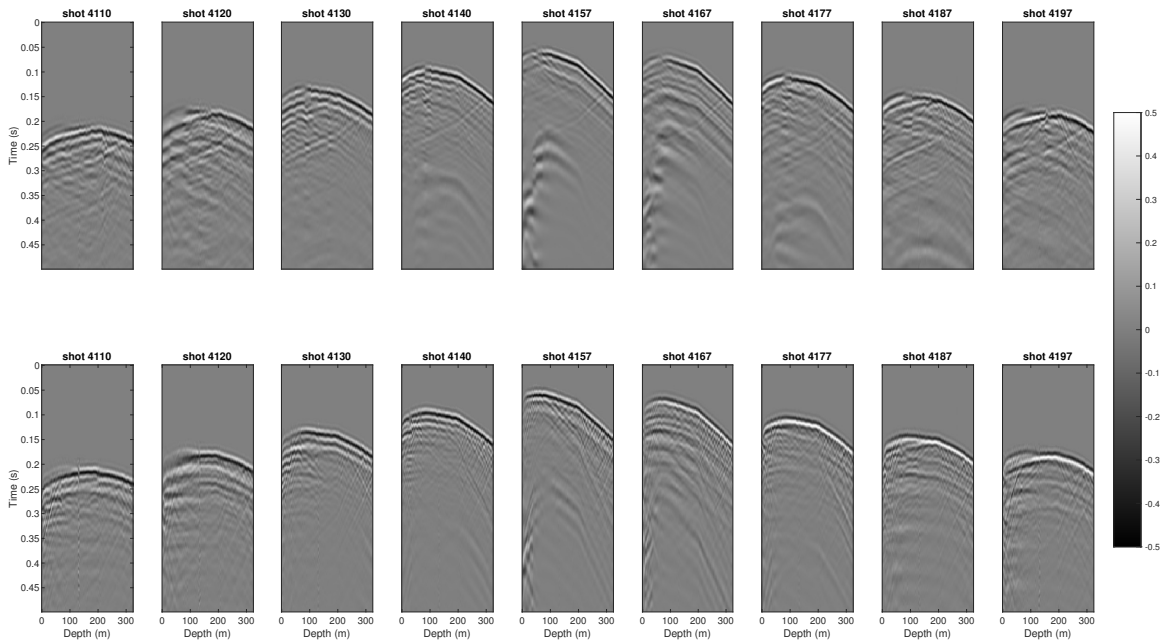

FIG. 3. The processed baseline data acquired in 2018: vertical component (top row) and Hmax component (bottom row).

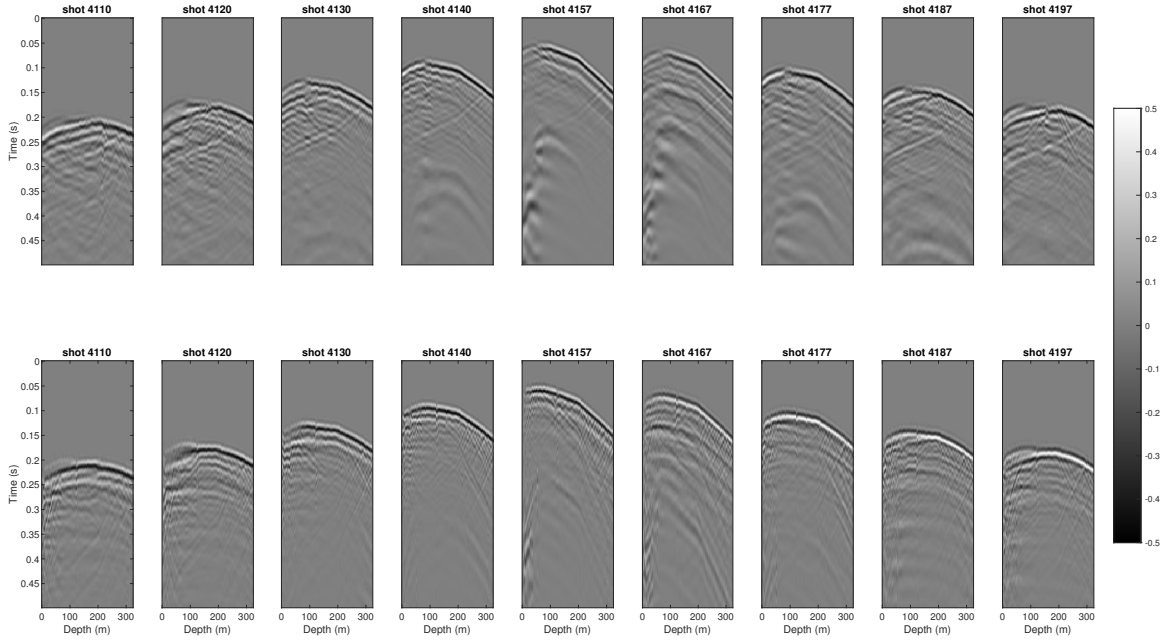

FIG. 4. The processed monitoring data acquired in 2022: vertical component (top row) and Hmax component (bottom row).

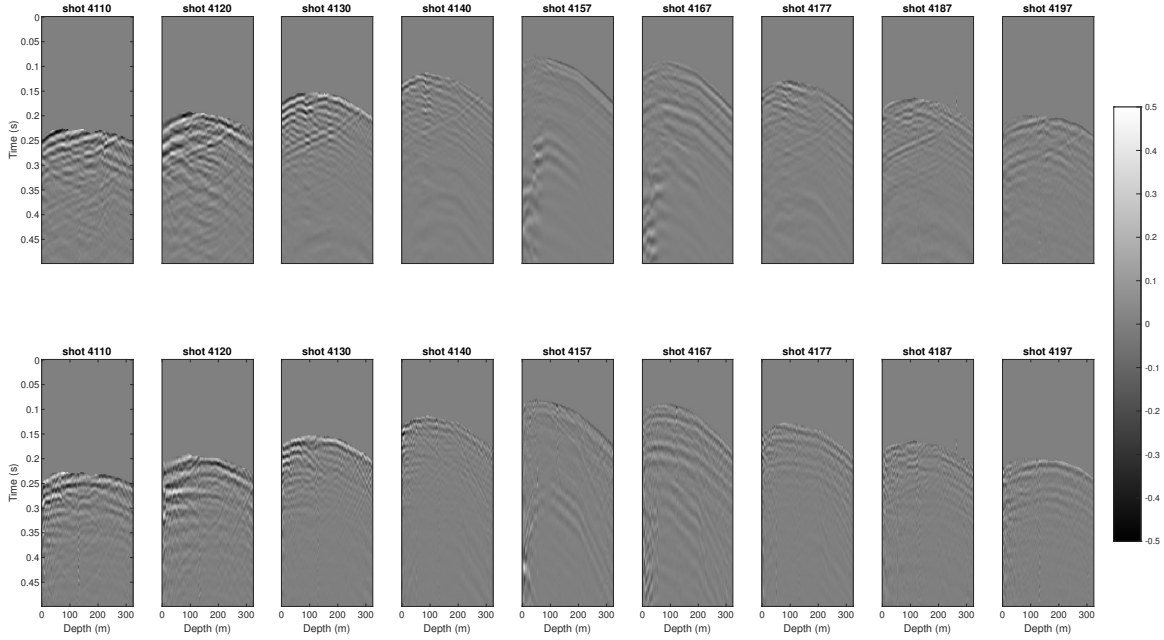

FIG. 5. The difference between monitoring data and baseline data: vertical component (top row) and Hmax component (bottom row).

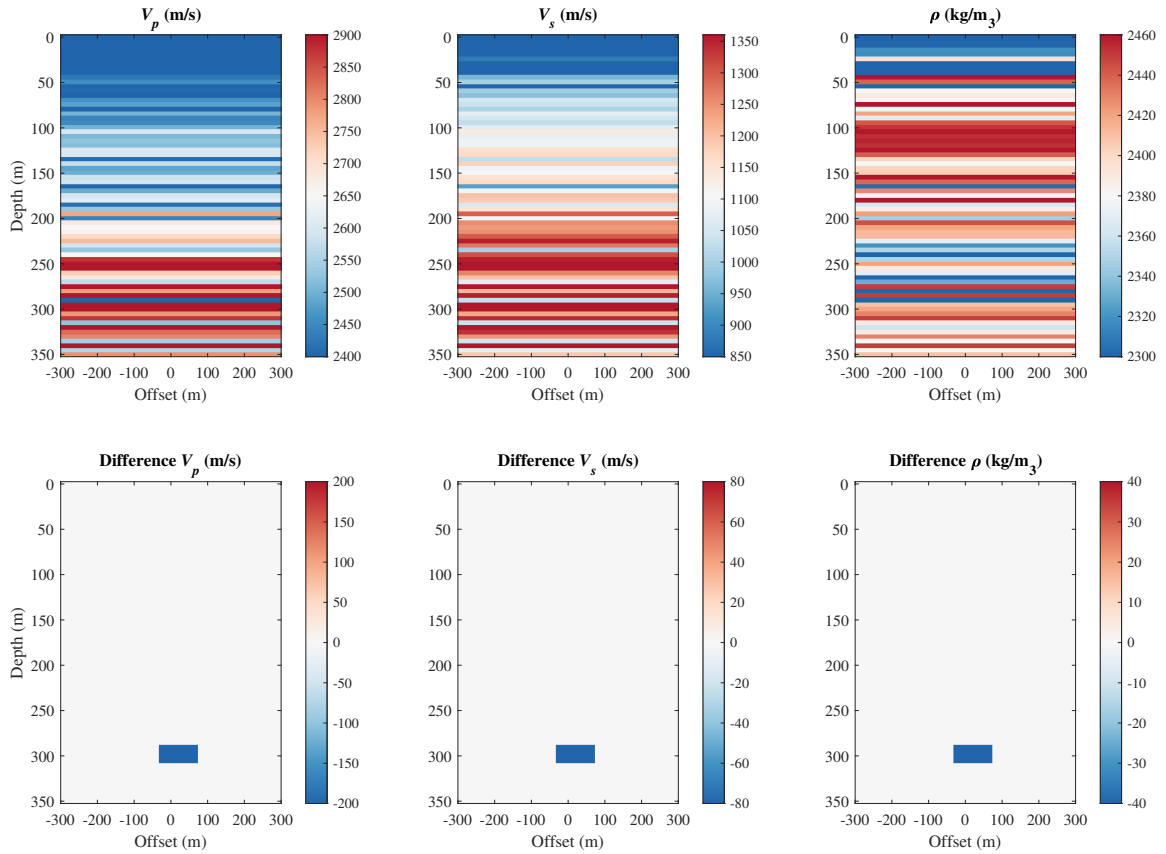

FIG. 6. The synthetic true model and time-lapse true model.

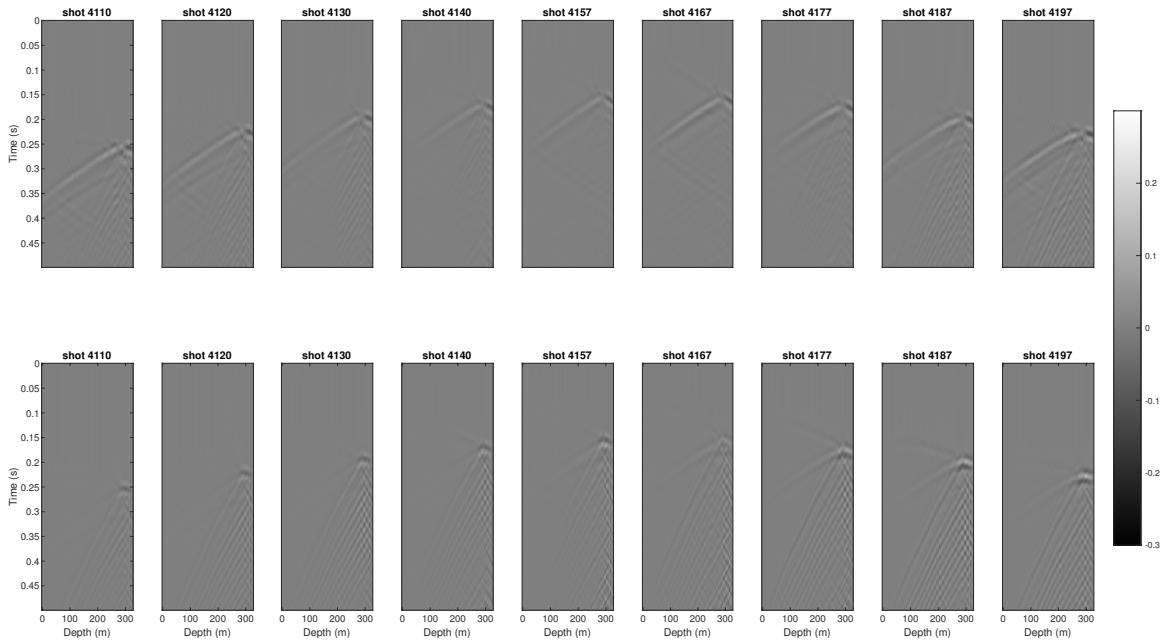

FIG. 7. The synthetic difference between monitoring data and baseline data: vertical component (top row) and Hmax component (bottom row).

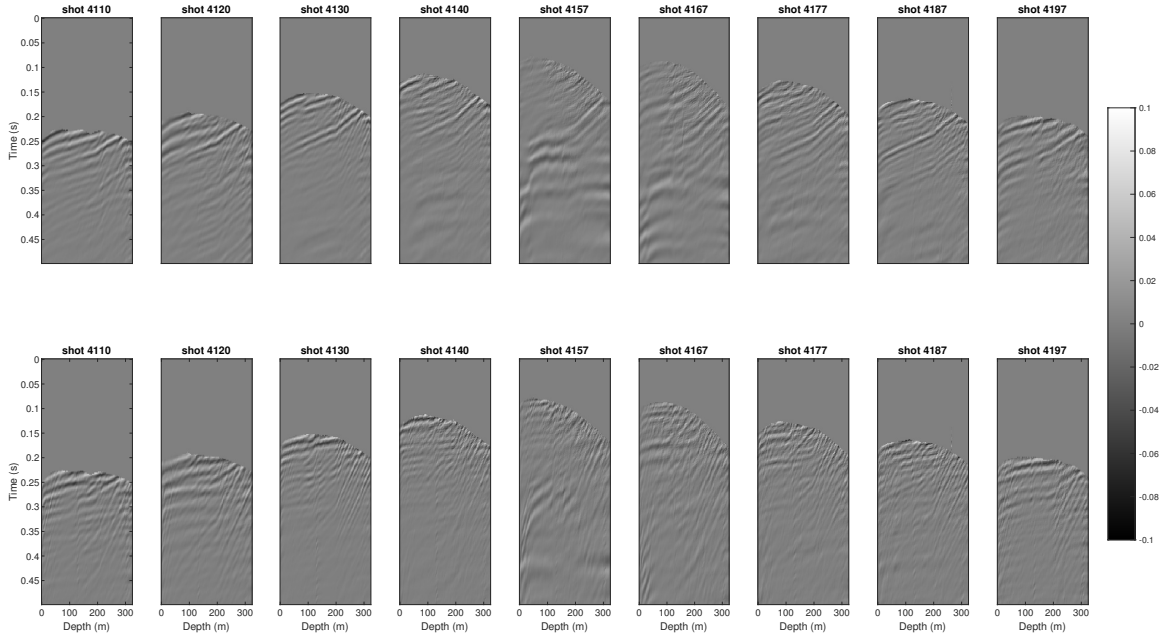

FIG. 8. The separated difference upgoing wavefield between monitoring data and baseline data: vertical component (top row), and Hmax component (bottom row).

Inversion

The selection of an appropriate parameterization holds crucial importance in multiparameter FWI. An analysis of scattering patterns caused by various irregularities suggests that the impedance-density parameterization suits smaller reflection angles. In comparison, the velocity-density parameterization is better suited for larger reflection angles and transmitted geometries—the velocity parameterization in VSP data FWI, considering that transmitted arrivals exhibit dominant energy(Roberts et al., 2008). Following a similar rationale, we choose to parameterize the inversion based on elastic parameters (V_{p}, V_{s}, and ρ).

The model size is 600 m in the x-direction and 330 m in the z-direction, and the space interval is 5 m. This report focuses on frequencies between 6 Hz and 75 Hz. For the inversion, we consider one frequency band consisting of 70 frequencies, from low to high frequencies. The inversion approach could be divided into two steps: the source-only inversion (effective source estimation schematic (Keating et al., 2021) based on baseline data and the model-only inversion for baseline and monitoring data. We consider an effective source (Keating et al., 2021) depth of 40 m to implement the effective sources inversion strategy. The inversion is performed with 50 iterations of limited-memory Broyden-Fletcher-Goldfarb-Shanno (LBFGS) optimization used at each band.

Figure 9 shows the inverted models for baseline data and time-lapse inverted models of V_{p}, V_{s}, and ρ. Figure 10 compares the initial and inverted velocities models with the well logs data. It can be seen that EFWI introduces much detail into very smooth starting models. The injection took place at a depth of 300 m. Inversion results for V_{p} in the vicinity of the well location show good agreement with the log data. The time-lapse anomaly

introduced by CO_2 sequestration is imaged successfully.

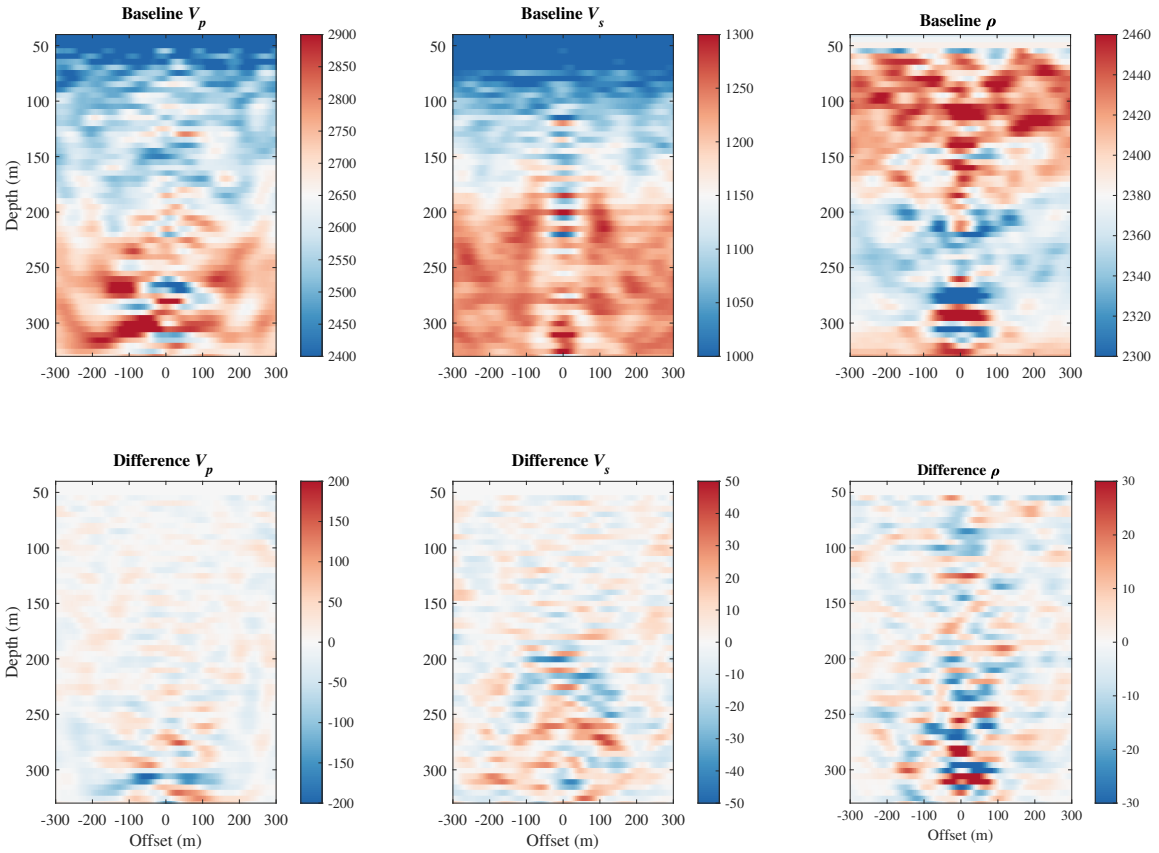

FIG. 9. The inverted baseline V_{p}, V_{s}, and ρ, models, and the inverted time-lapse V_{p}, V_{s}, and ρ, models .

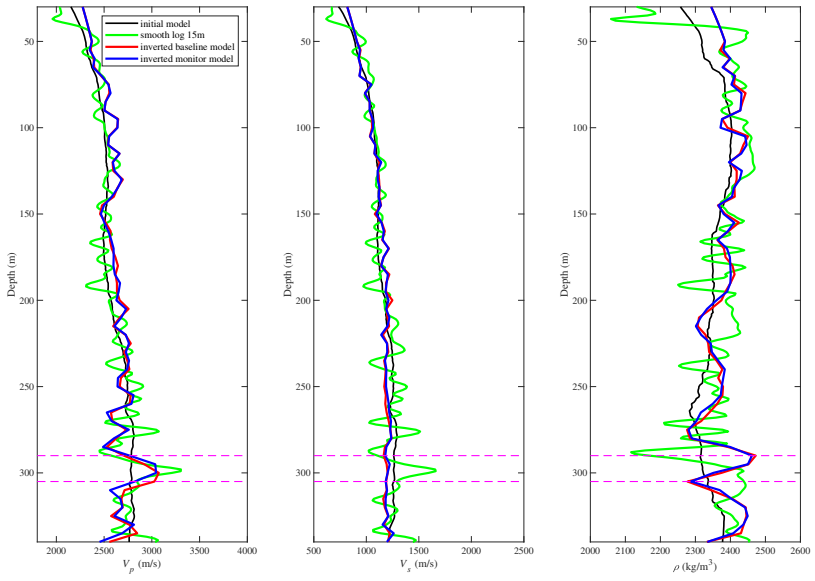

FIG. 10. The comparison of the initial and inverted baseline and monitoring velocities with the well logs data.

DISCUSSION AND CONCLUSIONS

The outcomes from conducting 2D ERTM on field VSP data demonstrate this technology's capability in delivering high-resolution subsurface physical properties models. It effectively identifies and quantifies anomalies within P-wave velocities. Specifically, our study detected a magnitude of V_{p} anomaly ranging between 130–210 m/s.

Upon comparing the field data inversion results with the well log data, it became evident that V_{p} displays a good match, while V_{s} and ρ exhibit a poorer match. This is possibly influenced by the initial inaccuracies in Vs caused by inaccurate predicted well log S-wave velocity data within shallow depths (0 - 223 meters). These inaccuracies likely contribute to the inadequate estimation of the initial V_{s} values, consequently affecting the final match with the actual field data.

ACKNOWLEDGMENTS

The sponsors of CREWES are gratefully thanked for continued support. This work was funded by CREWES industrial sponsors, NSERC (Natural Science and Engineering Research Council of Canada) through the grant CRDPJ 543578-19. This work was done in collaboration with the Carbon Management Canada.

REFERENCES

Charara, M., Barnes, C., and Tarantola, A., 1996, The state of affairs in inversion of seismic data: An ovsp example, *in* SEG Technical Program Expanded Abstracts 1996, Society of Exploration Geophysicists, 1999–2002.

Eaid, M. V., Keating, S. D., and Innanen, K. A., 2020, Multiparameter seismic elastic full-waveform inversion with combined geophone and shaped fiber-optic cable data: Geophysics, **85**, No. 6, R537–R552.

Egorov, A., Pevzner, R., Bóna, A., Glubokovskikh, S., Puzyrev, V., Tertyshnikov, K., and Gurevich, B., 2017, Time-lapse full waveform inversion of vertical seismic profile data: Workflow and application to the co2crc otway project: Geophysical Research Letters, **44**, No. 14, 7211–7218.

Hall, K. W., Bertram, K. L., Bertram, M., Innanen, K., and Lawton, D. C., 2019, Simultaneous accelerometer and optical fibre multi-azimuth walk-away vsp experiment: Newell county, alberta, canada, *in* SEG International Exposition and Annual Meeting, SEG, D043S111R007.

Hu, Q., Grana, D., and Innanen, K. A., 2023, Feasibility of seismic time-lapse monitoring of co2 with rock physics parametrized full waveform inversion: Geophysical Journal International, **233**, No. 1, 402–419.

Hu, Q., and Innanen, K., 2019, Rock physics analysis for the well-log data at CaMI FRS: CREWES Research Reports.

Innanen, K., Hall, K., and Lawton, D., 2022, A time-lapse multi-offset, multi-azimuth vsp acquired as a candidate for low-cost monitoring of co2 injection and storage: CREWES Research Reports.

Keating, S., Eaid, M., and Innanen, K., 2021, Effective sources: removing the near surface from the vsp fwi problem: CREWES Report.

Keating, S., and Innanen, K. A., 2019, Parameter crosstalk and modeling errors in viscoacoustic seismic full-waveform inversion: Geophysics, **84**, No. 4, R641–R653.

Owusu, J. C., Podgornova, O., Charara, M., Leaney, S., Campbell, A., Ali, S., Borodin, I., Nutt, L., and Menkiti, H., 2016, Anisotropic elastic full-waveform inversion of walkaway vertical seismic profiling data from the arabian gulf: Geophysical Prospecting, **64**, No. 1, 38–53.

Pan, W. Y., Innanen, K. A., Geng, Y., and Li, J. X., 2019, Interparameter trade-off quantification for isotropic-elastic full-waveform inversion with various model parameterizations: Geophysics, **84**, No. 2, R185–R206.

Roberts, M. A., Singh, S., and Hornby, B. E., 2008, Investigation into the use of 2d elastic waveform inversion from look-ahead walk-away vsp surveys: Geophysical prospecting, **56**, No. 6, 883–895.

Virieux, J., and Operto, S., 2009, An overview of full-waveform inversion in exploration geophysics: Geophysics, **74**, No. 6, WCC1–WCC26.